Journal of Photochemistry and Photobiology A: Chemistry 225 (2011) 8–16

Contents lists available at SciVerse ScienceDirect

Journal of Photochemistry and Photobiology A: Chemistry

journal homepage: www.elsevier.com/locate/jphotochem

Molecular design of triarylamine dyes incorporating phenylene spacer and the influence of alkoxy substituent on the performance of dye-sensitized solar cells

Hongyu Han, Mao Liang*, Kai Tang, Xiaobing Cheng, Xueping Zong, Zhe Sun, Song Xue*

Department of Applied Chemistry, Tianjin University of Technology, Tianjin 300384, PR China

ARTICLE INFO

Article history:
Received 23 June 2011
Received in revised form
11 September 2011
Accepted 22 September 2011
Available online 29 September 2011

Keywords:
Dye-sensitized solar cell
Photovoltaic
High molar extinction coefficient
Phenylene spacer

ABSTRACT

Molecular design and understanding the structure–property relationship of π-conjugated spacer play pivotal roles in realization of considerable enhancement performance of dye-sensitized solar cells (DSSCs). Three triphenylmaine dyes, namely **MX11-13**, have been designed and synthesized, which incorporate 2,2,6,6-tetramethylbenzo[1,2-*d*;4,5-*d*′]bis[1,3]dioxole (TMBD), phenyl and 1,4-dipropoxybenzene (DPB) as π-conjugated spacer, respectively. The effects of alkoxy substituent upon the photophysical, electro-chemical characteristics and performance of dye-sensitized solar cells are investigated. For a typical device, the **MX13**-based cell affords an overall power conversion efficiency (η) of 7.02%, with short-circuit photocurrent density (J_{SC}), open-circuit voltage (V_{OC}) and fill factor (*ff*) of 15.5 mA cm^{-2}, 697 mV and 0.65, respectively.

1. Introduction

There has been considerable interest for development of cheap and easily accessible renewable energy sources due to increasing energy demands and global warming. Compared to traditional silicon-based solar cells, dye-sensitized solar cells (DSSCs) are viewed as promising candidates for renewable clean energy sources in virtue of their low manufacturing cost and impressive photovoltaic performance [1]. The DSSCs composed of a mesoporous semiconductor metal semiconductor [2], photosensitizer [3], redox electrolyte [4], and a counter electrode are complex systems. To achieve high solar power conversion efficiency, therefore, great efforts are focused on designing and synthesizing new photosensitizers: Ru-based complexes and organic sensitizers. The former compounds contain expensive ruthenium metal and require careful synthesis and tricky purification steps. On the other hand, organic sensitizers with low cost, ease of structural tuning, and generally high molar extinction coefficients have emerged as competitive alternatives to the Ru-based counterparts [5]. As a result, various tailor-made organic dyes including coumarin [6,7], indoline [8], triphenylamine [9–15], dialkylaniline [16,17], bis(dimethylfluorenyl) aminophenyl [18,19], truxeneylaminophenyl [20–23] and carbazole1 [24,25] have been reported, showing promising power efficiency values in the range of 5–10.3%.

Most efficient metal-free organic sensitizers are constituted by donor (D), π-conjugated spacer (π) and acceptor moieties (A). The π-conjugated spacer between the donor and acceptor is recognized an important role in determining the overall conversion efficiency. Thiophene derivatives [9–15] and phenyl derivatives [26–28] have been incorporated as the conjugated spacer for tuning the wavelength ranges, absorption capability, and other characteristics required for DSSCs. It is noted that the effect of substituting groups of the chromophores on photovoltaic performance is distinguishable, apart from the impact of chromophore itself. A successful molecular engineering was achieved by incorporating long alkyl groups into the thiophene group, which not only increased the photocurrent but also minimized charge recombination [25]. Another successful substituting group is alkoxy groups. Using 3,4-ethylenedioxythiophene (EDOT) as π-conjugated spacer, which was connected to triphenylmaine or functional triarylamine, exhibited high photocurrent and high open-circuit photovoltage [21,22,29]. Very recently, Liang et al. reported **OR** dyes bearing 3,4-propylenedioxythiophene (ProDOT) linkers with enhanced performance for DSSCs [30]. These results could be mainly attributed to broadened absorption spectra and high molar extinction coefficients of organic dyes as a result of alkoxy substituent effect. In addition, the side chain of both EDOT and ProDOT is orbicular, guaranteeing the amount of dye-uptake on the TiO_2 film due to small size of the side chain.

However, this strategy of molecular design was not found in construction of phenylene spacer after a search of the literature. As part of our efforts to investigate the substituent effect of alkoxy groups, we designed and synthesized a

* Corresponding authors. Tel.: +86 22 60214250; fax: +86 22 60214252.
E-mail addresses: liangmao717@126.com (M. Liang), xuesong@ustc.edu.cn (S. Xue).

1010-6030/$ – see front matter © 2011 Elsevier B.V. All rights reserved.
doi:10.1016/j.jphotochem.2011.09.019

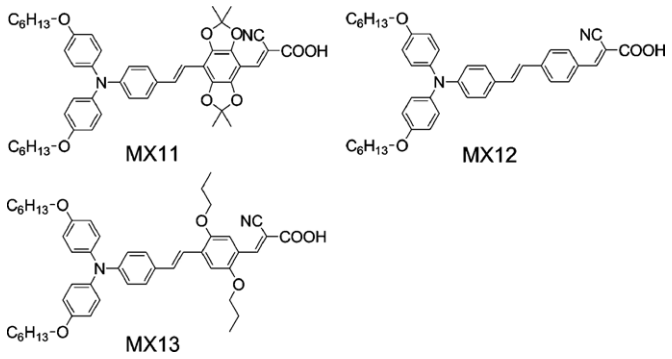

Scheme 1. Molecular structures of **MX11–13**.

new building block, namely 2,2,6,6-tetramethylbenzo[1,2-*d*;4,5-*d*′]bis[1,3]dioxole (TMBD), which shares attractive properties with EDOT/ProDOT such as high electron-richness and controlling dye aggregation arising from nonplanar three-dimensional (3D) branched structure. Herein we reported the synthesis and characterization of three triphenylmaine dyes, namely **MX11**, **MX12** and **MX13**, that incorporating TMBD, phenyl and 1,4-dipropoxybenzene (DPB) as π-conjugated spacer, respectively. In particular, the profound impacts of alkoxy substituent groups upon the photophysical, electro-chemical characteristics and performance of dye-sensitized solar cells were investigated. Molecular structures of these three dyes are shown in Scheme 1.

2. Experimental

2.1. Materials and instruments

The synthetic routes for dyes **MX11–13** are shown in Scheme 2. *n*-Butyllithium was purchased from Alfa. *N*,*N*-Dimethylformamide was dried over and distilled from CaH_2 under an atmosphere of nitrogen. Phosphorus oxychloride was freshly distilled before use. Dichloromethane and chloroform were distilled from calcium hydride under nitrogen atmosphere. Titanium(IV) isopropoxide, tertbutylpyridine and lithium iodide were purchased from Aldrich. All other solvents and chemicals used in this work were analytical grade and used without further purification.

^{1}H NMR and ^{13}C NMR spectra were recorded on a Bruker AM-400 spectrometer. The reported chemical shifts were against TMS. Mass spectra were recorded on a LCQ AD (Thermofinnigan, USA) mass spectrometer. The melting point was taken on a RY-1 thermometer and temperatures were uncorrected.

2.2. Photophysical and electrochemical measurements

The absorption spectra of the dyes either in solution or on the adsorbed TiO_2 films were measured by HITACHI U-3310 spectrophotometer. Adsorption of the dye on the TiO_2 surface was done by soaking the TiO_2 electrode in a mixture solution ethanol–dichloromethane 3:1 solution of the dye (standard concentration 3×10^{-4} M) at room temperature for 24 h. Fluorescence measurements were carried out with a HITACHI F-4500 fluorescence spectrophotometer. FT-IR spectra were obtained with a Bio-Rad FTS 135 FT-IR instrument.

Cyclic voltammetry measurements were performed at room temperature on a computer controlled LK2005A electrochemical workstation with Pt-wires as working electrode and counter electrode, Ag/AgCl electrode as reference electrode at a scan rate of 100 mV s^{-1}. Tetrabutylammonium perchlorate (TBAP, 0.1 mol/L) and MeCN were used as supporting electrolyte and solvent, respectively. The measurements were calibrated using ferrocene as standard. The redox potential of ferrocene internal reference is taken as 0.63 V vs NHE. Electrochemical impedance spectroscopy (EIS) in the frequency range of 100 mHz to 100 kHz was performed with a PARSTAT 2273 potentiostat/galvanostat/FRA in the dark with the alternate current amplitude set at 10 mV.

2.3. Fabrication of DSSCs

TiO_2 colloid was prepared according to the literature method [31], which was used for the preparation of the nanocrystalline films. The TiO_2 paste consisting of 18 wt.% TiO_2, 9 wt.% ethyl cellulose and 73 wt.% terpineol was firstly prepared, which was printed on a conducting glass (Nippon Sheet Glass, Hyogo, Japan, fluorine-doped SnO_2 over layer, sheet resistance of 10 Ω/sq) using a screen printing technique. The thickness of the TiO_2 film was controlled by selection of screen mesh size and repetition of printing. The film was dried in air at 120 °C for 30 min and calcined at 500 °C for 30 min under flowing oxygen before cooling to room temperature. The heated electrodes were impregnated with a 0.05 M titanium tetrachloride solution in a water-saturated desiccator at 70 °C for 30 min and fired again to give a ca. 10 μm thick mesoscopic TiO_2 film. The TiO_2 electrode was stained by immersing it into a dye solution containing 300 μM dye sensitizers (ethanol–dichloromethane 3:1) for 24 h at room temperature. Then the sensitized-electrode was rinsed with dry ethanol and dried by a dry air flow. Pt catalyst was deposited on the FTO glass by coating with a drop of H_2PtCl_6 solution (40 mM in ethanol) with the heat treatment at 395 °C for 15 min to give photoanode. The dye-covered TiO_2 electrode and Pt-counter electrode were assembled into a sandwich type cell according to the literature method [31]. The DSSCs had an active area of 0.16 cm^2 and electrolyte composed of 0.6 M 1,2-dimethyl-3-*n*-propylimidazolium iodide (DMPImI), 0.1 M LiI, 0.05 M I_2, and 0.5 M tertbutylpyridine in acetonitrile.

2.4. Characterization of DSSCs

The photocurrent–voltage (*J*–*V*) characteristics of the solar cells were carried out using a Keithley 2400 digital source meter controlled by a computer and a standard AM1.5 solar simulator Oriel 91160-1000 (300 W) SOLAR SIMULATOR 2 × 2 BEAM. The light intensity was calibrated by an Oriel reference solar cell. The action spectra of monochromatic incident photon-to-current conversion efficiency (IPCE) for solar cell were performed by using a commercial setup (QTest Station 2000 IPCE Measurement System, CROWNTECH, USA).

2.5. Computational methods

The geometrical structures of the three dyes were optimized by performed density functional theory (DFT) calculations and time-dependent DFT (TDDFT) calculations of the excited states at the B3LYP/6-31+G(d) level with the Gaussian 03W program package.

2.6. The detailed experimental procedures and characterization data

2.6.1. Synthesis of carbaldehyde ***2***

2,2,6,6-Tetramethyl-benzo[1,2-*d*;4,5-*d*′]bis[1,3]dioxole [32] (446 mg, 2 mmol) was added to a round bottom flask under nitrogen, followed by diethyl ether (25 mL) and TMEDA (1.0 mL, 6.6 mmol). A 2.2 M *n*-BuLi solution in hexane (3.0 mL, 6.6 mmol) was slowly added at room temperature. The solution was then brought to reflux for 1 h. After being re-cooled to room temperature, DMF (1.2 mL, 16 mmol) was slowly added to the cloudy solution. The colored solution was again brought to reflux for 2 h. The reaction was cooled to room temperature and 10 mL water

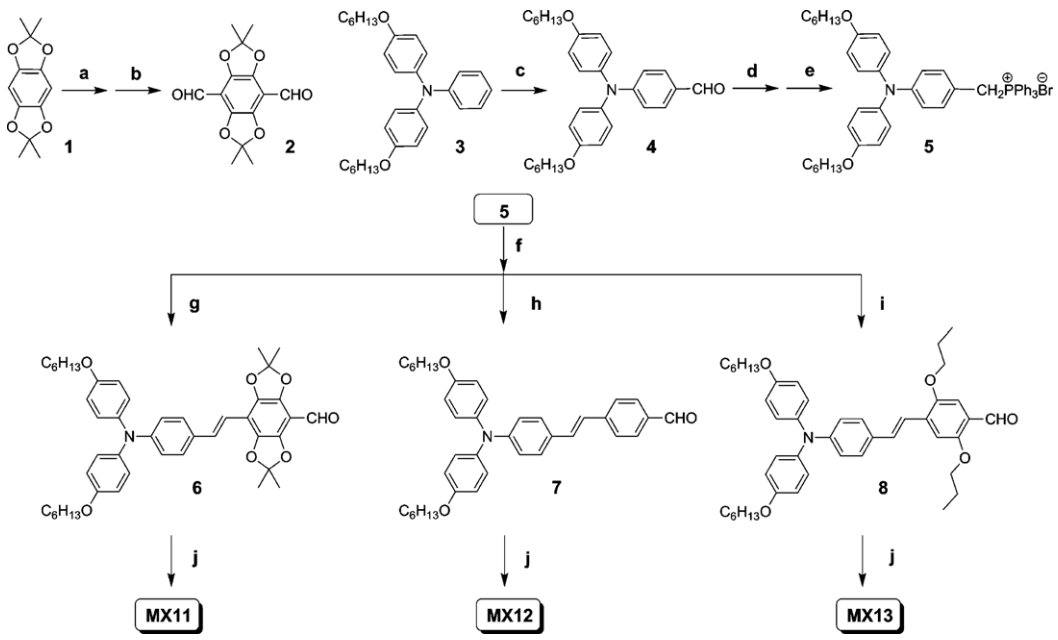

Scheme 2. Synthetic route toward the **MX11**–**13**. (a) TMEDA, *n*-BuLi, ether, reflux. (b) DMF, reflux. (c) DMF/$POCl_3$, 100 °C. (d) $NaBH_4$, EtOH, reflux. (e) PPh_3.HBr, $CHCl_3$, reflux. (f) Bu^tOK, THF, 0 °C, 30 min. (g) Carbaldehyde **2**, THF, reflux. (h) 1,4-Phthalaldehyde, THF, reflux. (i) 2,5-Dipropoxy-benzene-1,4-dicarbaldehyde, THF, reflux. (j) $CNCH_2COOH$, CH_3CN, piperidine, reflux.

was added. The aqueous layer was extracted by dichloromethane. The organic layer was combined and dried over $MgSO_4$. The solution was filtered and evaporated under reduced pressure to get a salmon pink solid. The solid was purified by column chromatography on silica gel (petroleum/ethyl acetate = 10:1 as the eluent) to yield a red solid (292 mg, 53%). Mp: 215–217 °C. IR (KBr): 2998, 2837, 2755, 1686, 1478, 1383, 1313, 1279, 1047 cm^{-1}. ^1H NMR ($CDCl_3$, 400 MHz): δ 10.12 (s, 2H), 1.77 (s, 12H). ^{13}C NMR ($CDCl_3$, 100 MHz): δ 185.1, 141.3, 122.5, 109.2, 25.9. HRMS (ESI) calcd for $C_{14}H_{14}O_6$ ($M+H^+$): 279.0868. Found: 279.0868.

2.6.2. Synthesis of carbaldehyde *4*

To a solution of compound **3** (1 g, 2.24 mmol) in anhydrous DMF (10 mL, 126 mmol) at 0 °C under nitrogen atmosphere was added $POCl_3$ (2 mL, 13.40 mmol) dropwise and stirred for 1 h. Subsequently, the mixture was heated at 90–100 °C for 2 h. The mixture was cooled and poured into an ice-water with vigorous stirring. After neutralization with NaOH, the mixture was extracted with ethyl acetate. The organic fractions were combined and dried over anhydrous $MgSO_4$. The resulting oil was purified by column chromatography on silica gel (petroleum:ethyl acetate = 10:1 as the eluent) to yield a bright yellow oil **4** (856 mg, 85.6%). IR (KBr): 2929, 2859, 1688, 1592, 1562, 1504, 1469, 1390, 1241, 1160, 1028, 826 cm^{-1}. ^1H NMR (400 MHz, $CDCl_3$): δ 9.75 (s, 1H), 7.63 (d, J = 8.00 Hz, 2H), 7.12 (d, J = 8.40 Hz, 4H), 6.89 (d, J = 8.40 Hz, 4H), 6.85 (d, J = 8.00 Hz, 2H), 3.96 (t, J = 6.32 Hz, 4H), 1.82–1.75 (m, 4H), 1.48–1.45 (m, 4H), 1.36–1.34 (m, 8H), 0.93 (t, J = 6.36 Hz, 6H). ^{13}C NMR (100 MHz, $CDCl_3$): δ 190.2, 157.0, 154.1, 138.6, 131.4, 128.0, 127.7, 116.7, 115.6, 68.4, 31.6, 29.4, 25.8, 22.6, 14.0. HRMS (ESI) calcd for $C_{31}H_{39}NO_3$ ($M+H^+$): 474.3008. Found: 474.3009.

2.6.3. Synthesis of triarylamine *5*

Carbaldehyde **4** (856 mg, 1.81 mmol) was added to a round bottom flask, followed by ethanol (15 mL) and $NaBH_4$ (137 mg, 3.62 mmol). Subsequently, the solution is then brought to reflux for 1 h. The reaction was cooled to room temperature and was quenched by saturated aqueous ammonium chloride solution. The aqueous layer was extracted with dichloromethane. The combined organic layers were washed with brine and then dried over $MgSO_4$. The solution was filtered, and concentrated in vacuo giving a crude oil. The oil was dissolved in 25 mL of anhydrous chloroform and PPh_3HBr (620 mg, 1.81 mmol) was added. The reaction was then brought to reflux for 1 h before being re-cooled to ambient temperature. The mixture was concentrated in vacuo to remove the solvent. The (4-(bis(4-(hexyloxy)phenyl)amino)benzyl)triphenylphosphonium bromide was obtained (1.448 g, 1.81 mmol) as a yellow oil.

2.6.4. Synthesis of carbaldehyde *6*

The compound **5** (2.50 g, 3.12 mmol) was dissolved in 30 mL of dry THF under N_2 atmosphere and cooled to 0 °C. Potassium tert-butoxide (349 mg, 3.12 mmol) was added slowly while stirring the solution vigorously. The generated red solution was stirred at 0 °C for another 30 min, and then brought to room temperature. After that, compound **2** (868 mg, 3.12 mmol) was added in portion and the mixture was heated to reflux for 5 h. The solution was poured into ice water and extracted with dichloromethane. The organic layer was washed with water and dried with $MgSO_4$. The product was obtained by a column chromatography (petroleum:ethyl acetate = 10:1 as the eluent) as a bright yellow solid (786 mg, 35%). Mp: 145–147 °C. IR (KBr): 3422, 2930, 2840, 1687, 1652, 1596, 1506, 1448, 1384, 1329, 1243, 1159, 1044, 1005, 831 cm^{-1}. ^1H NMR ($CDCl_3$, 400 MHz): δ 10.04 (s, 1H), 7.48 (d, J = 16.4 Hz, 1H), 7.35 (d, J = 8.4 Hz, 2H), 7.06 (d, J = 8.8 Hz, 4H), 6.89 (d, J = 8.4 Hz, 2H), 6.86 (d, J = 8.8 Hz, 4H), 6.84 (d, J = 16.4 Hz, 1H), 3.95 (t, J = 6.5 Hz, 4H), 1.80–1.75 (m, 16H), 1.48–1.45 (m, 4H), 1.36–1.34 (m, 8H), 0.92 (t, J = 6.6 Hz, 6H). ^{13}C NMR ($CDCl_3$, 100 MHz): δ 185.1, 155.8, 149.2, 140.7, 140.3, 138.2, 135.9, 129.0, 127.8, 126.8, 120.1, 119.8, 115.3, 114.3, 112.8, 104.6, 76.7, 68.3, 31.6, 30.92, 29.3, 25.9, 25.8, 22.6, 14.0. HRMS (ESI) calcd for $C_{45}H_{53}NO_7$ ($M+H^+$): 720.3900. Found: 720.3905.

2.6.5. Synthesis of *MX11*

To a solution of compound **6** (100 mg, 0.14 mmol) and cyanoacetic acid (16 mg, 0.19 mmol) was added acetonitrile (5 mL), dichlormethane (2.5 mL) and piperidine (100 μL). The solution was

refluxed for 5 h. After cooling the solution, the solvent was removed in vacuo. Dichloromethane was added. The organic layer was separated and washed 3 times with water, dried over anhydrous $MgSO_4$, and filtered. The pure product was obtained by silica gel chromatography (dichloromethane:methanol = 10:1 as the eluent) to give a red powder (76 mg, 69.0%). Mp: 187 – 189 °C. IR (KBr): 3422, 2918, 2849, 1593, 1566, 1506, 1241, 1150, 1120, 1021, 800 cm^{-1}. ^1H NMR (400 MHz, $CDCl_3$): δ 7.79 (s, 1H), 7.33 (d, J = 8.7 Hz, 2H), 7.31 (d, J = 16.0 Hz, 1H), 7.00 (d, J = 8.7 Hz, 4H), 6.88 (d, J = 8.8 Hz, 4H), 6.75 (d, J = 16.0 Hz, 1H), 6.72 (d, J = 8.5 Hz, 1H), 3.95 (t, J = 6.6 Hz, 4H), 2.17 (s, 2H), 1.80–1.75 (m, 16H), 1.48–1.45 (m, 4H), 1.36–1.34 (m, 8H), 0.92 (t, J = 6.6 Hz, 6H). ^{13}C NMR (100 MHz, DMSO): δ 156.0, 149.0, 140.7, 140.0, 138.7, 136.1, 128.1, 127.5, 119.8, 119.1, 116.0, 115.9, 79.6, 68.2, 67.5, 31.5, 29.2, 26.0, 25.7, 22.5, 14.3. HRMS (ESI) calcd for $C_{48}H_{54}N_2O_8$ ($M+H^+$): 787.3958. Found: 787.3953.

2.6.6. Synthesis of carbaldehyde **7**

The product was synthesized according to the procedure for synthesis of **6**; yield 30%. IR (KBr): 3434, 2928, 2363, 1685, 1590, 1506, 1473, 1240, 1072 cm^{-1}. ^1H NMR (DMSO, 400 MHz): δ 9.93 (s, 1H), 7.83 (d, J = 16.4 Hz, 2H), 7.73 (d, J = 8.6 Hz, 2H), 7.43 (d, J = 8.4 Hz, 2H), 7.37 (d, J = 16.4 Hz, 1H), 7.11 (d, J = 16.4 Hz, 1H), 6.99 (d, J = 8.6 Hz, 4H), 6.87 (d, J = 8.6 Hz, 4H), 6.73 (d, J = 8.6 Hz, 2H), 3.89 (t, J = 5.6 Hz, 4H), 1.69–1.59 (m, 4H), 1.39–1.35 (m, 4H), 1.31–1.26 (m, 8H), 0.91 (t, J = 6.6 Hz, 6H). ^{13}C NMR (DMSO, 100 MHz): δ 192.5, 167.4, 156.0, 149.2, 144.2, 139.9, 135.0, 132.3, 132.2, 131.9, 130.5, 129.1, 128.4, 127.4, 126.9, 124.5, 119.0, 115.9, 68.1, 65.5, 31.8, 30.5, 29.5, 25.7, 22.4, 19.1, 14.3, 14.0. HRMS (ESI) calcd for $C_{39}H_{45}NO_3$ ($M+H^+$): 576.3477. Found: 576.3481.

2.6.7. Synthesis of ***MX12***

The product was synthesized according to the procedure for synthesis of **MX11**, giving a salmon pink powder in 64.0% yield. Mp: 187–189 °C. IR (KBr): 3416, 1664, 1499, 1438, 1390, 1111, 559 cm^{-1}. ^1H NMR (400 MHz, DMSO): δ 7.89 (s, 1H), 7.87 (d, J = 8.4 Hz, 2H), 7.65 (d, J = 8.4 Hz, 2H), 7.45 (d, J = 8.7 Hz, 2H), 7.31 (d, J = 16.3 Hz, 1H), 7.09 (d, J = 16.3 Hz, 1H), 7.03 (d, J = 8.8 Hz, 4H), 6.92 (d, J = 8.8 Hz, 4H), 6.75 (d, J = 8.7 Hz, 2H), 3.95 (t, J = 6.4 Hz, 4H), 1.73 – 1.66 (m, 4H), 1.43 – 1.37 (m, 4H), 1.32 – 1.28 (m, 8H), 0.89 (t, J = 6.8 Hz, 6H). ^{13}C NMR (100 MHz, DMSO): δ 163.6, 155.9, 148.9, 147.0, 140.4, 140.0, 132.3, 130.6, 130.3, 128.8, 128.2, 127.4, 126.8, 124.9, 120.1, 119.3, 116.0, 68.1, 39.4, 31.5, 29.2, 25.7, 22.5, 14.4. HRMS (ESI) calcd for $C_{42}H_{46}N_2O_4$ ($M+H^+$): 643.3536. Found: 643.3530.

2.6.8. Synthesis of carbaldehyde ***8***

The product was synthesized according to the procedure for synthesis of **6**; yield 28%. IR (KBr): 2932, 2871, 1728, 1590, 1505, 1240 cm^{-1}. ^1H NMR (DMSO, 400 MHz): δ 10.31 (s, 1H), 7.47 (d, J = 16.2 Hz, 1H), 7.44 (s, 1H), 7.39 (d, J = 8.6 Hz, 2H), 7.25 (d, J = 16.2 Hz, 1H), 7.18 (s, 1H), 7.03 (d, J = 8.6 Hz, 4H), 6.91 (d, J = 8.6 Hz, 4H), 6.75 (d, J = 8.6 Hz, 2H), 4.13 (t, J = 6.3 Hz, 2H), 3.97–3.89 (m, 6H), 1.79–1.75 (m, 4H), 1.67–1.61 (m, 4H), 1.41–1.34 (m, 4H), 1.30–1.27 (m, 8H), 1.03–0.98 (m, 6H), 0.92–0.85 (m, 6H). ^{13}C NMR (DMSO, 100 MHz): δ 188.4, 167.4, 156.3, 156.0, 150.2, 149.1, 139.9, 135.1, 133.1, 132.2, 132.0, 129.1, 128.2, 127.5, 123.4, 119.1, 115.9, 111.2, 110.1, 70.8, 70.5, 68.1, 65.5, 31.5, 30.9, 29.2, 25.7, 22.3, 19.1, 14.4, 14.0, 13.4, 11.0. HRMS (ESI) calcd for $C_{45}H_{57}NO_5$ ($M+H^+$): 692.4315. Found: 692.4314.

2.6.9. Synthesis of ***MX13***

The product was synthesized according to the procedure for synthesis of MX11, giving a fuchsia powder in 55.0% yield. Mp: 193–196 °C. IR (KBr): 3422, 2929, 2362, 1637, 1508, 1385, 1072 cm^{-1}. ^1H NMR (400 MHz, DMSO): δ 8.51 (s, 1H), 7.4 (d, J = 16.4 Hz, 1H), 7.38 (d, J = 8.4 Hz, 2H), 7.36 (s, 1H), 7.25 (d, J = 16.4 Hz, 1H), 7.15 (d, 1H), 7.00 (d, J = 8.7 Hz, 4H), 6.88 (d, J = 8.7 Hz, 4H), 6.73 (d, J = 8.4 Hz, 2H), 4.08 (t, J = 6.3 Hz, 2H), 3.94–3.87 (m, 6H), 1.80–1.74 (m, 4H), 1.68-1.61 (m, 4H), 1.37–1.35 (m, 4H), 1.28–1.20 (m, 8H), 1.01 – 0.98 (m, 6H), 0.87 – 0.84 (m, 6H). ^{13}C NMR (100 MHz, DMSO): δ 164.5, 157.2, 156.0, 153.4, 149.8, 149.1, 145.9, 139.9, 138.2, 132.6, 132.1, 132.0, 131.9, 129.1, 128.9, 127.5, 119.8, 116.2, 111.7, 110.3, 70.9, 70.6, 68.2, 53.0, 31.8, 29.5, 25.7, 22.6, 22.5, 22.5, 14.3, 11.1. HRMS (ESI) calcd for $C_{48}H_{58}N_2O_6$ ($M+H^+$): 759.4373. Found: 759.4366.

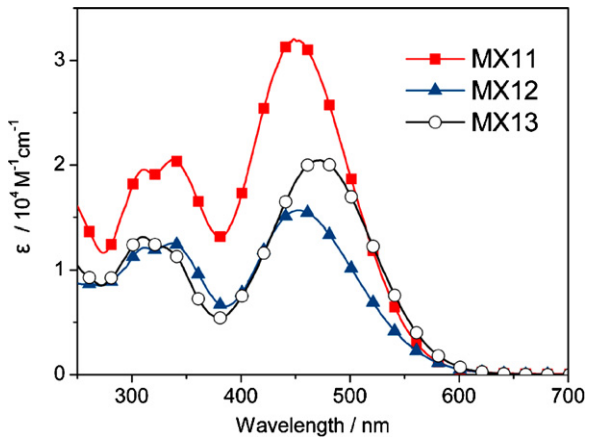

Fig. 1. Absorption spectra of **MX11–13** in CH_2Cl_2 (1×10^{-5} M).

3. Results and discussion

3.1. UV–vis absorption/emission spectra

As Fig. 1 presents, we first recorded the UV–vis absorption spectra of **MX11–13** dissolved in dichloromethane so as to preliminarily evaluate the substituent influence on the light capture capacity, and the detailed parameters are summarized in Table 1. The three dyes display two strong absorption bands at around 280–380 nm and 400–600 nm, which mainly stem from the intramolecular charge-transfer transition. **MX11** featuring four alkoxy substituents on the pheneylene has a maximum molar absorption coefficient (ε) of 55×10^3 M^{-1} cm^{-1}, which is remarkably higher than the corresponding value of **MX12** (21×10^3 M^{-1} cm^{-1}) and **MX13** (32×10^3 M^{-1} cm^{-1}) in the visible region. The maximum absorption coefficient dependence on molecular structure is pronounced. In general, those possessing electron donor groups on the spacer displayed high values of ε, while those possessing withdrawing groups displayed low values [33]. It is evident that the maximum molar absorption coefficient of organic dyes is enhanced with the increasing alkoxy substituent groups. The maximum absorption peaks (λ_{max}) of **MX11–13** were observed in visible region at 453, 453 and 472 nm, respectively. The maximum absorption peak dependence on dye structure is also pronounced. Those possessing large conjugation length [34] or large extent of electron delocalization [35] displayed high maximum absorption peaks. The geometry of molecular structure plays an important role in the absorption peak as well [30,36]. Minor changes in the geometry of molecular structure may result in different electron delocalization. For the **MX12** and **MX13**, the dihedral angles of phenylene spacer and cyanoacetic acid are 3.4° and 1.5° (Fig. 2), respectively, resulting in similar planar conjugating system. Therefore, a red shift of **MX13** relative to **MX12** is mainly derived from more delocalization over an entire conjugated system due to alkoxy substituent groups. In the case of **MX11**, the dihedral angle between the TMBD and cyanoacetic acid is 45.8° (Fig. 2), giving a more twisted configuration than that of **MX12-13**. If there are no alkoxy substituent groups on the phenylene spacer, **MX11** will exhibit a blue-shifted

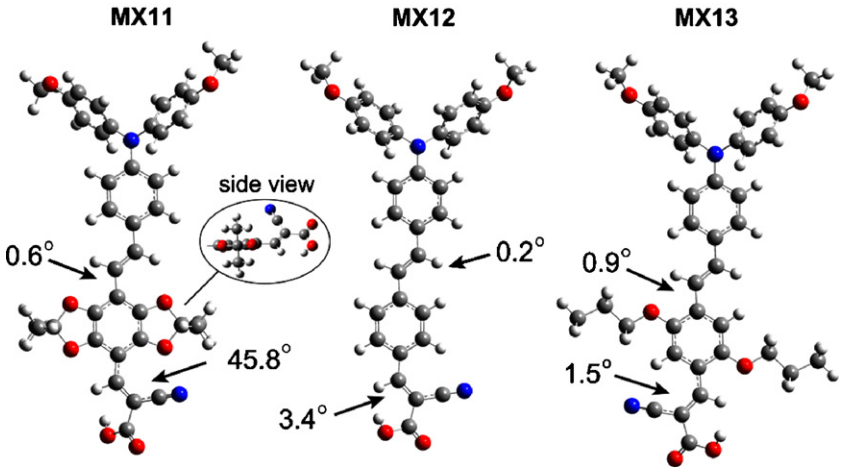

Fig. 2. Optimized geometrical configuration of **MX11–13**.

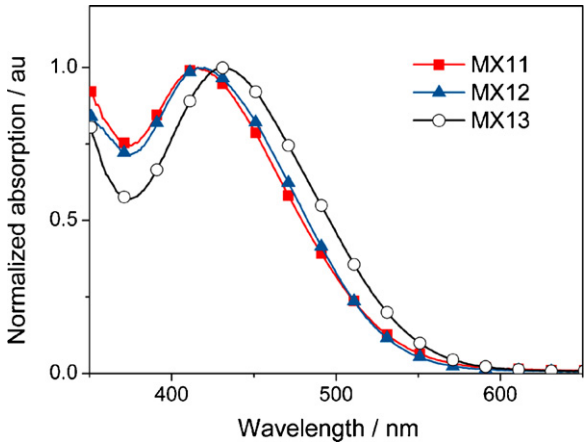

Fig. 3. Absorption spectra of **MX11–13** on TiO_2 film.

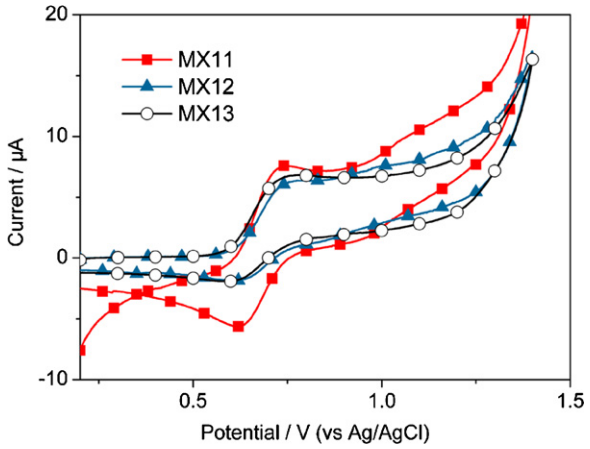

Fig. 4. Cyclic voltammogram of **MX11–13**.

absorption relative to **MX12**. However, the maximum absorption peak of **MX11** is the same as that of **MX12**. This result indicated that extent of electron delocalization is enhanced with increased alkoxy substituent groups on the phenylene spacer. Therefore, the introduction of alkoxy substituent groups in π spacer favors the light harvesting of organic dyes.

Upon adsorption onto transparent mesoporous TiO_2 films (3 μm), **MX11–13** show an evident hypsochromic effect compared with that measured in solution (Fig. 3), indicating a weaker electron-withdrawing capability of the carboxylatetitanium assembly than that of the carboxylic acid [37]. Emission maxima of dyes **MX11–13** can be found at 500–700 nm when the dyes are excited at their respective absorption bands at 400–600 nm (Table 1).

3.2. Electrochemical properties

To obtain and understand the molecular orbital energy levels, cyclic voltammetry (CV) was employed to measure the ground-state oxidation potential (E_{ox}) of the dyes in acetonitrile solution. Representative cyclic voltammograms are shown in Fig. 4. The first quasi-reversible one-electron oxidation wave is taken as the highest occupied molecular orbital (HOMO) level. The excited-state potential (E_{ox^*}), reflecting the LUMO level of the dye, can be derived from the ground-state oxidation potential and the zero–zero excitation energy (E_{0-0}) according to the following equation: $E_{ox^*} = E_{ox} - E_{0-0}$. As depicted in Table 1, the HOMO levels of dyes **MX11** and **13** (0.81 V vs NHE) are lower than that of **MX12** (0.83 V vs NHE) because of the presence of the

Table 1
Optical properties and electrochemical properties of three dyes.

Dye	λ_{max}/nm ($\varepsilon/10^3$ M^{-1} cm^{-1})[a]	λ_{max}/nm[b]	λ_{int}/nm[c]	E_{0-0}/eV[d]	E_{ox}/V[e]	E_{ox^*}/V[f]
MX11	453 (37)	605	541	2.29	0.81	−1.48
MX12	453 (14)	626	537	2.31	0.83	−1.48
MX13	472 (21)	620	556	2.23	0.81	−1.42

[a] Absorption spectra of dyes measured in DCM (1.0×10^{-5} M).
[b] Emission spectra of dyes measured in DCM (1.0×10^{-5} M)
ε is the extinction coefficient at λ_{max} of absorption.
[c] The intersect of the normalized absorption and the emission spectra (λ_{int}).
[d] E_{0-0} values were calculated from: $E_{0-0} = 1240/\lambda_{int}$.
[e] E_{ox} (vs NHE) of the dyes in acetonitrile was measured by cyclic voltammogram.
[f] E_{ox^*} (vs NHE) was calculated from $E_{ox^*} = E_{ox} - E_{0-0}$.

Table 2
Photovoltaic performance of DSSCs sensitized with the three dyes.[a]

Dye	J_{SC}/mA cm^{-2}	V_{OC}/mV	*ff*	η/%
MX11	10.6	681	0.67	4.84
MX12	15.0	720	0.64	6.91
MX13	15.5	697	0.65	7.02

[a] Photovoltaic performances of DSSCs were measured under irradiation of AM1.5G simulated solar light (100 mW cm^{-2}) at room temperature with a 0.16 cm^2 working area.

electron-donating alkoxy substituent groups. They are all more positive than the Nernst potential of I^-/I_3^- redox couple (0.4 V vs NHE), ensuring regeneration of the oxidized dyes by I^- after electron injection. The LUMO levels of **MX13** (−1.42 V vs NHE) is more positive than that of dyes **MX11** and **MX12** (−1.48 V vs NHE), narrowing the HOMO–LUMO energy gaps and resulting in red shift of absorption spectra. They are all negative than the conduction band of TiO_2 (E_{CB}, −0.5 V vs NHE), which provided sufficient driving forces for electron injection. Therefore, the HOMO–LUMO levels of **MX11**–**13** are suitable for DSSCs.

3.3. Photovoltaic performance

The incident monochromatic photon-to-current conversion efficiency (IPCE) measurements of DSSCs based on **MX11**–**13** using the redox electrolyte consisting of 0.6 M DMPImI, 0.05 M I_2, 0.1 M LiI, and 0.5 M TBP in acetonitrile are shown in Fig. 5. The IPCE spectra of **MX12** and **MX13** exceed 75% in the visible spectral region from 400 to 580 nm, reaching their maximum of 84% and 82% at 480–500 nm, respectively. Considering the light absorption and scattering loss by the conducting glass, the broad and high photocurrent action spectrum indicates high light harvesting yield in these devices [34]. **MX13** exhibits a slightly broader IPCE absorption relative to **MX12**, which is in good accord with the preceding absorption measurements. **MX11** containing TMBD unit exhibits a relatively lower IPCE relative to those of the **MX12**–**13**.

Photovoltaic characteristics of the DSSCs based on the three dyes under AM1.5G condition (100 mW cm^{-2}) are displayed in Table 2 and the *J*–*V* curves are plotted in Fig. 6. The short-circuit photocurrent densities (J_{SC}), open-circuit photovoltages (V_{OC}), and fill factors (*ff*) of DSSCs sensitized by **MX12** and **MX13** are 15.0 mA cm^{-2}, 720 mV, 0.64 and 15.5 mA cm^{-2}, 697 mV, 0.65, respectively, yielding overall conversion efficiencies (η) up to 6.91% and 7.02%, respectively. We attribute the excellent efficiencies to both broad and high IPCE spectra of **MX12** and **MX13**. Under the same

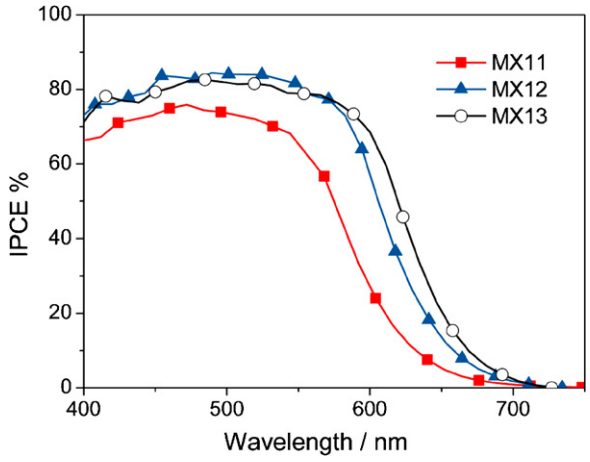

Fig. 5. IPCE spectra for DSSCs based on **MX11**–**13**.

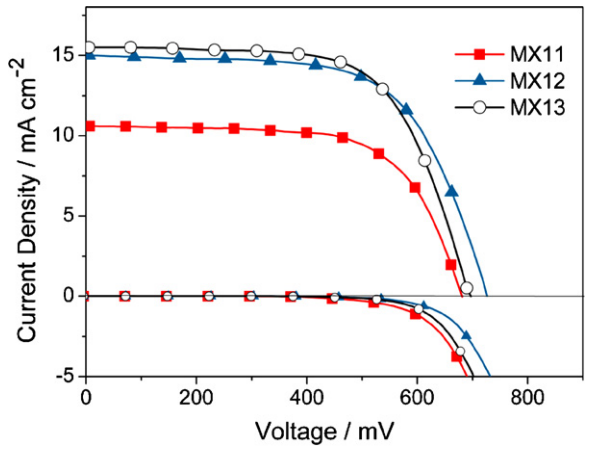

Fig. 6. Current–potential (*J*–*V*) curves for the DSSCs based on **MX11**–**13** under AM1.5 irradiation (top) and in the dark (bottom).

conditions, **MX11** gave J_{SC} of 10.6 mA cm^{-2}, V_{OC} of 681 mV, and *ff* of 0.67, corresponding η of 4.84%.

3.4. Dependence of short-circuit photocurrent densities on the interfacial charge recombination, LUMO levels and dye aggregation.

As shown in above, the substituent effect of alkoxy groups on photovoltaic performance of DSSCs are obvious. When the pheneyl is displaced by DBP containing two alkoxy groups, the J_{SC} rises to 15.5 mA cm^{-2}, leading to a higher efficiency of **MX13**. In contrast, introduction of TMBD as spacer (**MX11**) does not lead to a further enhanced J_{SC} (10.6 mA cm^{-2}) relative to that of **MX13**. To comprehend the significant J_{SC} variation, factors contributing to IPCE need to be considered. IPCE is expressed by the light harvesting efficiency (LHE) and product of absorbed photon-to-current conversion efficiency (APCE) [38]:

$$\mathrm{IPCE}(\lambda) = \mathrm{LHE} \times \mathrm{APCE} = \mathrm{LHE} \times \eta_{col} \times \Phi_{inj}$$

where APCE should be divided into two terms: the overall charge collective efficiency (η_{col}) and the overall electron injection efficiency (Φ_{inj}).

Light-harvesting efficiency: The LHE at the maximum absorption wavelength can be estimated using the following equation [39]: $\mathrm{LHE} = 1 - 10^{-A}$. Where *A* is the absorbance of the dye on TiO_2 at the maximum wavelength. According to our measurements, all the *A* values for the three dyes on the TiO_2 film (10 μm) are over 3, indicating similar LHE values for these dyes. Therefore, any difference in the photocurrent among DSSCs based on these dyes could be attributed to the difference of η_{col} and Φ_{inj}. Several factors including the interfacial charge recombination, LUMO levels and dye aggregation were discussed to scrutinize the overall charge collective efficiency and the overall electron injection efficiency in DSSCs, which could make a critical contribution to the IPCE summit.

Charge collection efficiency: To probe the possible impact of alkoxy substituents upon the interfacial charge recombination at the TiO_2/dye/electrolyte interface, the electrochemical impedance spectroscopy (EIS) is measured for the DSSCs based on the three dyes. Typical EIS Nyquist plots and Bode phase plots measured in the dark under a forward bias of −0.7 V are shown in Fig. 7. The equivalent circuit [22] presented in Fig. 7 was used to fit the experimental data of all of the samples. *Rs* are the series resistance accounting for the transport resistance of the TCO and the electrolyte. $C\mu$ and R_{CT} are the chemical capacitance and the charge recombination resistance at the TiO_2/electrolyte interface, respectively. C_{Pt} and R_{Pt} are the interfacial capacitance and charge

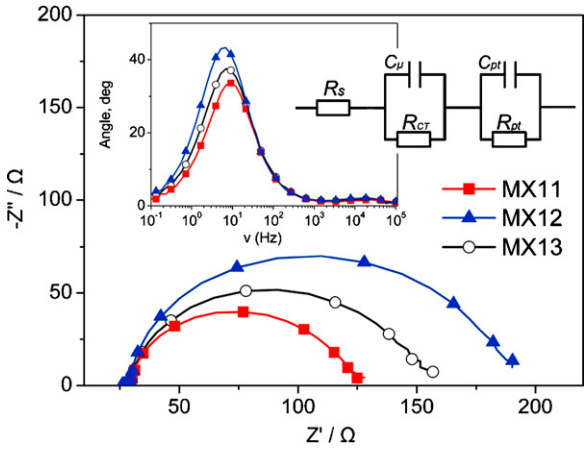

Fig. 7. EIS for DSSCs based on **MX11–13** measured in the dark under −0.7 V bias displayed in the form of Nyquist plots and Bode phase plots (insert); top right corner is the equivalent circuit used to fit the impedance spectra.

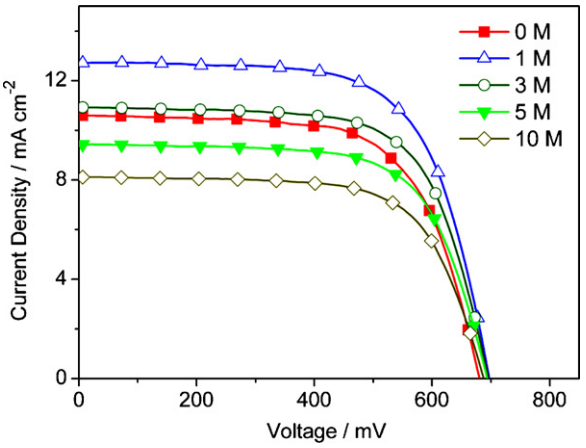

Fig. 9. *J–V* curves of DSSCs sensitized by **MX11** containing different concentration of CDCA as coadsorbent under AM1.5 irradiation.

transport resistance at the Pt/electrolyte interface, respectively. The larger semicircle at lower frequencies represents the R_{CT} at the TiO_2/dye/electrolyte interface. The fitted R_{CT} increases in the order of **MX11** (54 Ω) < **MXD13** (82 Ω) < **MXD12** (151 Ω), which is consistent with the sequence of V_{OC} values in the devices. In the range of potentials studied (Fig. 8), the fitted R_{CT} also increases in the order of **MX11** < **MXD13** < **MXD12**. The smaller R_{CT} value means the electron recombination from the conduction band to the electrolyte occurring more easily. This result can be cross-checked by measuring the *J–V* characteristics of the DSSCs in the dark (Fig. 6). Clearly, electron recombination in device will decrease the η_{col}, thus leading to lower IPCE. Therefore, the limited η_{col} in device based on **MX11** is one of the reasons for the lower IPCE.

These results also indicate that recombination of conduction band electrons to the electrolyte occurs more easily upon the substitution with the alkoxy groups. In a study on the V_{OC} of DSSCs using ruthenium dyes, O'Regan et al. have shown that a change of oxygen to sulfur in two equivalent positions in a Ru-based dye structure gives a 2-fold increase in the recombination rate and a 20–30 mV loss in V_{OC} [40]. Their results strongly support that binding of iodine to the dye is a key element of the recombination process in DSSCs. In a study of interfacial electron-transfer kinetics in metal-free organic dye-sensitized solar cells, Mori et al. supposed that the indirect electrostatic attraction of I_3^- by negatively charged atoms in the dyes (e.g., N atom in the cyanoacrylic acid group) increases the local concentration of I_3^- in the vicinity of TiO_2, facilitating dark reaction [41]. Although

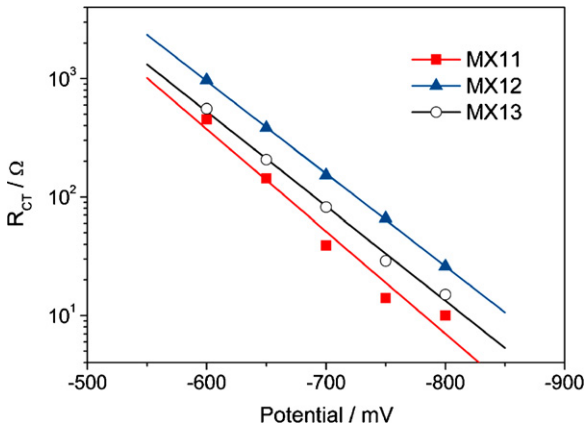

Fig. 8. Interfacial charge transfer resistance R_{CT} fitted from impedance spectra under a series of applied potentials.

we have not been able to show the iodine binding to oxygen, according to the results of EIS and dark line, it seems that there is an electrostatic attraction of I_3^- by oxygen atoms in **MX11** and **MXD13**, leading to a faster charge recombination reaction relative to **MX12**.

Electron injection efficiency: It is known that, an insufficient driving force for electron injection is possible to induce poor Φ_{inj}. LUMO levels of **MX11**, **MX12** and **MX13** are estimated to be −1.48, −1.48, and −1.42 V vs NHE, respectively (Table 1). We find that the driving forces for electron injection ($E_{ox^*} - E_{CB}$) are very similar for **MX11** and **MX12**, but the two dyes show quite different IPCE maxima. Furthermore, the two dyes have identical binding groups and similar electronic structure, suggesting that electronic coupling to CB states will be similar [42]. Therefore, it is not the LUMO level that limits the IPCE of **MX11**.

To estimate the dye aggregation on TiO_2 film, we have measured the amounts adsorbed on the TiO_2 film. By comparing the absorbance change of a dye solution (300 μM) before and after dye up-taking with a titania film, the surface coverages (Γ) of **MX11**, **MX12** and **MX13** anchored on TiO_2 film were determined to be 5.08×10^{-10}, 2.29×10^{-10} and 2.12×10^{-10} mol cm^{-2}, respectively. More intense light-absorption could be expected since the adsorption amount of **MX11** is about 2.1-fold higher than that of **MX12** and **MX13**. However, the IPCE maximum of **MX11** is fell behind that of **MX12** and **MX13**, which could be attributable to disadvantageous intermolecular energy transfer as a result of aggregate formation [30,43,44]. It seems that intermolecular π–π interaction in **MX11** is stronger than that in **MX12** and **MX13**, which may arise from the large rigid conjugation structure of TMBD.

It is well known that unfavorable dye aggregation on the semiconductor surface could be avoided through optimization of the molecular structure of the dye or by addition of coadsorbers (i.e. chenodeoxycholic acid (CDCA)) that prevent aggregation and enhance the Φ_{inj} [43]. The effect of CDCA concentration in the dye bath on the performance of **MX11**-based DSSCs was investigated by raising [CDCA] from the originally employed 1–10 mM (Fig. 9). Upon coadsorption with 1 mM CDCA, the J_{SC} increased from 10.6 to 12.7 mA cm^{-2}, resulting in accordingly improved η values (6.02%). The increased J_{SC} is attributed to enhancing Φ_{inj} resulting from relatively independent dye molecules arraying on TiO_2 surface. When [CDCA] exceeded 3 mM, the J_{SC} dropped continuously because of the decreasing of the dye adsorption amount. Under the same conditions, CDCA has no obvious influence on the J_{SC} of DSSCs based on **MX12** and **MX13** (1 mM CDCA, **MX12**: J_{SC} = 15.3 mA cm^{-2}; **MX13**: J_{SC} = 15.6 mA cm^{-2}). Though the optimized efficiency of **MX11** is still fell bellow the efficiency of **MX12** and **MX13**, it could be

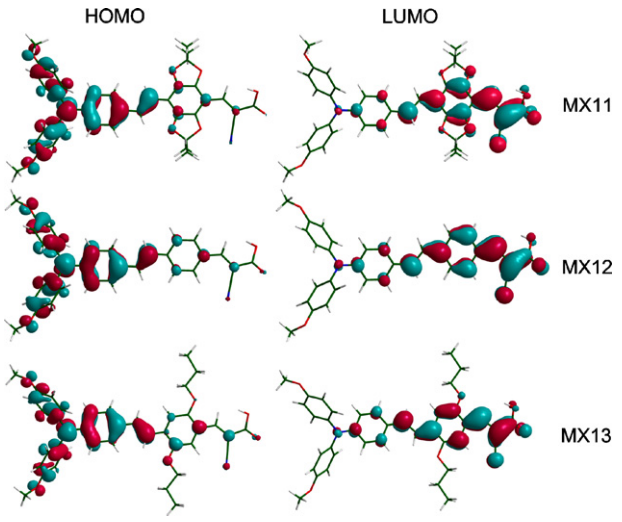

Fig. 10. Isodensity surface plots of the HOMO and LUMO of **MX11–13**.

concluded that the dye aggregation is one of the main reasons for lower electron injection efficiency of **MX11**.

3.5. Calculation analysis of dye structure

In order to obtain the geometrical configuration and characteristic features of the electronic structure of **MX11–13**, density functional theory (DFT) calculations were made on a B3LYP/6-31G level. We optimized the molecular structure of **MX11–13** in vacuo. The isodensity surface plots of HOMO (the highest occupied molecular orbital) and LUMO (the lowest unoccupied molecular orbital) are presented in Fig. 10. For the three dyes, the HOMO is delocalized throughout the entire molecule, with maximum components on the triphenylamine; and the LUMO is delocalized across the TMBD (or DPB, phenyl) and cyanoacrylic groups, indicating that the HOMO–LUMO excitation moves the electron distribution from the triarylamine to the cyanoacrylic acid moiety, thus allowing an efficient photoinduced electron transfer from the dye to the TiO_2 electrode under light irradiation. It is noted that, in spite of a more twisted configuration of **MX11**, the HOMO–LUMO excitation that moves the electron distribution from the triarylamine to the cyanoacrylic acid moiety is not broken, suggesting the effective intramolecular electron transfer in **MX11**.

4. Conclusions

In summary, a new series of triphenylmaine dyes, namely **MX11**, **MX12** and **MX13**, that incorporating TMBD, phenyl and DPB as π-conjugated spacer, respectively, were designed and synthesized. The effect of alkoxy substituent groups on the photophysical, electro-chemical characteristics and performance of dye-sensitized solar cells were investigated. Introduction of alkoxy substituent groups on phenyl enhances the electron-donating ability of spacer, which is beneficial to light-harvesting, such as enhancing the molar extinction coefficients and broaden absorption spectra. EIS and dark current measurements show that recombination of conduction band electron to the electrolyte occurs more easily upon the substitution with the alkoxy groups. Among the three dyes, **MX13** showed the highest efficiency of 7.02%, with a J_{SC} of 15.5 mA cm^{-2}, V_{OC} of 697 mV, and *ff* of 0.65. The J_{SC} of **MX11** is lower than that of **MX12** and **MX13** due to the limitation of collective efficiency over solar cell and electron injection efficiency, which is resulted from the charge recombination reaction and the dye aggregations, respectively. These results provide useful information for future rational design of metal-free organic dyes.

Acknowledgments

We are grateful to the National 863 Program (2009AA05Z421), the National Natural Science Foundation of China (21003096) and the Tianjin Natural Science Foundation (09JCZDJC24400) for financial supports.

References

[1] B. O'Regan, M. Grätzel, A low-cost high-efficiency solar cell based on dye-sensitized colloidal TiO_2 film, Nature 353 (1991) 737–739.
[2] Y. Chen, E. Stathatos, D.D. Dionysiou, Sol–gel modified TiO_2 powder films for high performance dye-sensitized solar cells, J. Photochem. Photobiol. A: Chem. 203 (2009) 192–198.
[3] Z. Kong, H. Zhou, J. Cui, T. Ma, X. Yang, L. Sun, A new class of organic dyes based on acenaphthopyrazine for dye-sensitized solar cells, J. Photochem. Photobiol. A Chem. 213 (2010) 152–157.
[4] R. Patel, J.A. Seo, J.H. Koh, J.H. Kim, Y.S. Kang, Dye-sensitized solar cells employing amphiphilic poly(ethylene glycol) electrolytes, J. Photochem. Photobiol. A Chem. 217 (2011) 169–176.
[5] A. Mishra, M.K.R. Fischer, P. Bäuerle, Metal-free organic dyes for dye-sensitized solar cells: from structure–property relationships to design rules, Angew. Chem.: Int. Ed. 48 (2009) 2474–2499.
[6] K. Hara, Y. Dan-oh, C. Kasada, Y. Ohga, A. Shinpo, S. Suga, K. Sayama, H. Arakawa, Effect of additives on the photovoltaic performance of coumarin-dye-sensitized nanocrystalline TiO_2 solar cells, Langmuir 20 (2004) 4205–4210.
[7] Z.S. Wang, Y. Cui, K. Hara, Y. Dan-oh, C. Kasada, A. Shinpo, A high-light-harvesting-efficiency coumarin dye for stable dye-sensitized solar cells, Adv. Mater. 19 (2007) 1138–1141.
[8] T. Horiuchi, H. Miura, K. Sumioka, S. Uchida, High efficiency of dye-sensitized solar cells based on metal-free indoline dyes, J. Am. Chem. Soc. 126 (2004) 12218–12219.
[9] D.P. Hagberg, J.-H. Yum, H. Lee, F.D. Angelis, T. Marinado, K.M. Karlsson, R. Humphry-Baker, L. Sun, A. Hagfeldt, M. Grätzel, M.K. Nazeeruddin, Molecular engineering of organic sensitizers for dye-sensitized solar cell applications, J. Am. Chem. Soc. 130 (2008) 6259–6266.
[10] G. Li, K.-J. Jiang, Y.-F. Li, S.-L. Li, L.-M. Yang, J. Phys. Chem. C 112 (2008) 11591; Z. Ning, Q. Zhang, W. Wu, H. Pei, B. Liu, H. Tian, Starburst triarylamine based dyes for efficient dye-sensitized solar cells, J. Org. Chem. 73 (2008) 3791–3797.
[11] A. Baheti, P. Tyagi, K.R.J. Thomas, Y.-C. Hsu, J.T. Lin, Simple triarylamine-based dyes containing fluorene and biphenyl linkers for efficient dye-sensitized solar cells, J. Phys. Chem. C 113 (2009) 8541–8547.
[12] L. Zhang, Y. Liu, Z. Wang, M. Liang, Z. Sun, S. Xue, Synthesis of sensitizers containing donor cascade of triarylamine and dimethylarylamine moieties for dye-sensitized solar cells, Tetrahedron 66 (2010) 3318–3325.
[13] M.-F. Xu, R.-Z. Li, N. Pootrakulchote, D. Shi, J. Guo, Z.-H. Yi, S.M. Zakeeruddin, M. Grätzel, P. Wang, Energy-level and molecular engineering of organic D–π–A sensitizers in dye-sensitized solar cells, J. Phys. Chem. C 112 (2008) 19770–19776.
[14] W.-D. Zeng, Y.-M. Cao, Y. Bai, Y.-H. Wang, Y.-S. Shi, M. Zhang, F.-F. Wang, C.-Y. Pan, P. Wang, Efficient dye-sensitized solar cells with an organic photosensitizer featuring orderly conjugated ethylenedioxythiophene and dithienosilole blocks, Chem. Mater. 22 (2010) 1915–1925.
[15] M. Liang, W. Xu, F. Cai, P. Chen, B. Peng, J. Chen, Z. Li, New triphenylamine-based organic dyes for efficient dye-sensitized solar cells, J. Phys. Chem. C 111 (2007) 4465–4472.
[16] K. Hara, M. Kurashige, S. Ito, A. Shinpo, S. Suga, K. Sayama, H. Arakawa, Novel polyene dyes for highly efficient dye-sensitized solar cells, Chem. Commun. 25 (2003) 2–53.
[17] T. Kitamura, M. Ikeda, K. Shigaki, T. Inoue, N.A. Anderson, X. Ai, T. Lian, S. Yanagida, Phenyl-conjugated oligoene sensitizers for TiO_2 solar cells, Chem. Mater. 16 (2004) 1806–1812.
[18] S. Kim, J.K. Lee, S.O. Kang, J. Ko, J.-H. Yum, S. Frantacci, F.D. Angelis, D.D. Censo, M.K. Nazeeruddin, M. Grätzel, Molecular engineering of organic sensitizers for solar cell applications, J. Am. Chem. Soc. 128 (2006) 16701–16707.
[19] H. Choi, C. Baik, S.O. Kang, J. Ko, M.-S. Kang, M.K. Nazeeruddin, M. Grätzel, Highly efficient and thermally stable organic sensitizers for solvent-free dye-sensitized solar cells, Angew. Chem.: Int. Ed. 47 (2008) 327–330.
[20] Z. Ning, Q. Zhang, H. Pei, J. Luan, C. Lu, Y. Cui, H. Tian, Photovoltage improvement for dye-sensitized solar cells via cone-shaped structural design, J. Phys. Chem. C 113 (2009) 10307–10313.
[21] M. Liang, M. Lu, Q. Wang, W. Chen, H. Han, Z. Sun, S. Xue, Efficient dye-sensitized solar cells with triarylamine organic dyes featuring functionalized-truxene unit, J. Power Sources 196 (2011) 1657–1664.
[22] M. Lu, M. Liang, H. Han, Z. Sun, S. Xue, Organic dyes incorporating bis-hexapropyltruxeneamino moiety for efficient dye-sensitized solar cells, J. Phys. Chem. C 115 (2011) 274–281.
[23] S. Lin, Y. Hsu, J.T. Lin, C. Lin, J. Yang, Isotruxene-derived cone-shaped organic dyes for dye-sensitized solar cells, J. Org. Chem. 75 (2010) 7877–7886.
[24] N. Koumura, Z.-S. Wang, S. Mori, M. Miyashita, E. Suzuki, K. Hara, Alkyl-functionalized organic dyes for efficient molecular photovoltaics, J. Am. Chem. Soc. 128 (2006) 14256–14257.

[25] Z.-S. Wang, N. Koumura, Y. Cui, M. Takahashi, H. Sekiguchi, A. Mori, T. Kubo, A. Furube, K. Hara, Hexylthiophene-functionalized carbazole dyes for efficient molecular photovoltaics: tuning of solar-cell performance by structural modification, Chem. Mater. 20 (2008) 3993–4003.
[26] H. Im, S. Kim, C. Park, S. Jang, C. Kim, K. Kim, N. Park, C. Kim, High performance organic photosensitizers for dye-sensitized solar cells, Chem. Commun. 133 (2010) 5–37.
[27] S. Hwang, J. Lee, C. Park, H. Lee, C. Kim, C. Park, M. Lee, W. Lee, J. Park, K. Kim, N. Park, C. Kim, A highly efficient organic sensitizer for dye-sensitized solar cells, Chem. Commun. 488 (2007) 7–89.
[28] D. Chen, Y. Hsu, H. Hsu, B. Chen, Y. Lee, H. Fu, M. Chung, S. Liu, H. Chen, Y. Chi, P. Chou, Organic dyes with remarkably high absorptivity; all solid-state dye sensitized solar cell and role of fluorine substitution, Chem. Commun. 525 (2010) 6–58.
[29] W. Liu, I. Wu, C. Lai, C. Lai, P. Chou, Y. Li, C. Chen, Y. Hsu, Y. Chi, Simple organic molecules bearing a 3,4-ethylenedioxythiophene linker for efficient dye-sensitized solar cells, Chem. Commun. 515 (2008) 2–54.
[30] Y. Liang, B. Peng, J. Liang, Z. Tao, J. Chen, Triphenylamine-based dyes bearing functionalized 3,4-propylenedioxythiophene linkers with enhanced performance for dye-sensitized solar cells, Org. Lett. 12 (2010) 1204–1207.
[31] S. Ito, T.N. Murakami, P. Comte, P. Liska, C. Grätzel, M.K. Nazeeruddin, M. Grätzel, Fabrication of thin film dye sensitized solar cells with solar to electric power conversion efficiency over 10%, Thin Solid Films 516 (2008) 4613–4619.
[32] T. Reddy, T. Iwama, H. Halpern, V. Rawal, general synthesis of persistent trityl radicals for EPR imaging of biological systems, J. Org. Chem. 67 (2002) 4635–4639.
[33] Y.J. Chang, T.J. Chow, Highly efficient triarylene conjugated dyes for sensitized solar cells, J. Mater. Chem. 21 (2011) 9523–9531.
[34] M. Xu, S. Wenger, H. Bala, D. Shi, R. Li, Y. Zhou, S. Zakeeruddin, M. Grätzel, P. Wang, Tuning the energy level of organic sensitizers for high-performance dye-sensitized solar cells, J. Phys. Chem. C 113 (2009) 2966–2973.
[35] W. Wu, J. Yang, J. Hua, J. Tang, L. Zhang, Y. Long, H. Tian, Efficient and stable dye-sensitized solar cells based on phenothiazine sensitizers with thiophene units, J. Mater. Chem. 20 (2010) 1772–1779.
[36] S. Paek, H. Choi, H. Choi, C.W. Lee, M.S. Kang, K. Song, M.K. Nazeeruddin, J. Ko, Molecular engineering of efficient organic sensitizers incorporating a binary π-conjugated linker unit for dye-sensitized solar cells, J. Phys. Chem. C 114 (2010) 14646–14653.
[37] D. Zhou, N. Cai, H. Long, M. Zhang, Y. Wang, P. Wang, An energetic and kinetic view on cyclopentadithiophene dye-sensitized solar cells: the influence of fluorine vs ethyl substituent, J. Phys. Chem. C 115 (2011) 3163–3171.
[38] X. Wang, H. Tamiaki, L. Wang, N. Tamai, O. Kitao, H.S. Zhou, S. Sasaki, Chlorophyll-a derivatives with various hydrocarbon ester groups for efficient dye-sensitized solar cells: static and ultrafast evaluations on electron injection and charge collection processes, Langmuir 26 (2010) 6320–6327.
[39] Z.-S. Wang, T. Yamaguchi, H. Sugihara, H. Arakawa, Significant efficiency improvement of the black dye-sensitized solar cell through protonation of TiO_2 films, Langmuir 21 (2005) 4272–4276.
[40] B.C. O'Regan, K. Walley, M. Juozapavicius, A. Anderson, F. Matar, T. Ghaddar, S.M. Zakeeruddin, C. Klein, J.R. Durrant, Structure/function relationships in dyes for solar energy conversion: a two-atom change in dye structure and the mechanism for its effect on cell voltage, J. Am. Chem. Soc. 131 (2009) 3541–3548.
[41] M. Miyashita, K. Sunahara, T. Nishikawa, Y. Uemura, N. Koumura, K. Hara, A. Mori, T. Abe, E. Suzuki, S. Mor, Interfacial electron-transfer kinetics in metal-free organic dye-sensitized solar cells: combined effects of molecular structure of dyes and electrolytes, J. Am. Chem. Soc. 130 (2008) 17874–17881.
[42] T. Marinado, D.P. Hagberg, M. Hedlund, T. Edvinsson, E.M.J. Johansson, G. Boschloo, H. Rensmo, T. Brinck, L.C. Sun, A. Hagfeldt, Rhodanine dyes for dye-sensitized solar cells: spectroscopy energy levels and photovoltaic performance, Phys. Chem. Chem. Phys. 11 (2009) 133–141.
[43] W. Zhu, Y. Wu, S. Wang, W. Li, X. Li, J. Chen, Z. Wang, H. Tian, Organic D–A–π–A solar cell sensitizers with improved stability and spectral response, Adv. Funct. Mater. 21 (2011) 756–763.
[44] Z.S. Wang, K. Hara, Y. Dan-Oh, C. Kasada, A. Shinpo, S. Suga, H. Arakawa, H. Sugihara, Photophysical and (photo)electrochemical properties of a coumarin dye, J. Phys. Chem. B 109 (2005) 3907–3914.